Computers and Concrete, Vol. 10, No. 6 (2012) 663-681
DOI: http://dx.doi.org/10.12989/cac.2012.10.6.663

Plastic hinge length of circular reinforced concrete columns

Yu-Chen Ou*, Raditya Andy Kurniawan, Dimas Pramudya Kurniawan and Nguyen Dang Nguyen

Department of Construction Engineering, National Taiwan University of Science and Technology, Taipei, Taiwan

(Received December 21, 2010, Revised May 4, 2012, Accepted June 9, 2012)

Abstract. This paper presents a parametric study of the plastic hinge length of circular reinforced concrete columns using a three-dimensional finite element analysis method, and using the Taguchi robust design method to reduce computational cost. Parameters examined include the longitudinal reinforcing ratio, the shear span-to-depth ratio, the axial force ratio and the concrete compressive strength. The study considers longitudinal reinforcement with yield strengths of 414 MPa and 685 MPa, and proposes simplified formulas for the plastic hinge length of circular reinforced concrete columns, showing that increases in plastic hinge length correlate to increases in the axial load, longitudinal reinforcing and shear span-to-depth ratios. As concrete strength increases, the plastic hinge length decreases for the 414 MPa case but increases for the 685 MPa case.

Keywords: reinforced concrete columns; plastic hinge length; Taguchi method; finite element analysis.

1. Introduction

When a column is subjected to large earthquake loading, the end region of the column may experience significant inelastic rotation. The inelastic rotation results in inelastic curvature that is distributed nonlinearly over the region. For convenience in calculation, the inelastic curvature is assumed to be constant over a length referred to as plastic hinge length. Plastic hinge length is a critical parameter for seismic analysis and the design of reinforced concrete structures. Several studies have suggested various formulas to estimate the plastic hinge length. Eqs. (1)-(5) are proposed, respectively, by Baker and Amarakone (1964), Corley (1966), Mattock (1967), Paulay and Priestley (1992) and Bae and Bayrak (2008).

$$L_p = 0.8k_1k_3\left(\frac{L}{d}\right)c \tag{1}$$

$$L_p = \frac{d}{2} + 0.2\frac{L}{\sqrt{d}} \tag{2}$$

$$L_p = \frac{d}{2} + 0.05L \tag{3}$$

* Corresponding author, Associate Professor, E-mail: yuchenou@mail.ntust.edu.tw

$$L_p = 0.08L + 0.022 d_b f_y \ (f_y \text{ in MPa}) \tag{4}$$

$$\frac{L_p}{h} = \left[0.3\left(\frac{P}{P_0}\right) + 3\left(\frac{A_s}{A_g}\right) - 0.1\right]\left(\frac{L}{h}\right) + 0.25 \geq 0.25 \tag{5}$$

where L_p=plastic hinge length; k_1=coefficient related to type of steel (mild or cold work steel); k_3= coefficient related to concrete strength; d=effective beam depth; L=distance from the critical section to the point of contra-flexure; c=neutral axis depth at ultimate condition; d_b=diameter of longitudinal reinforcement; f_y=yield strength of longitudinal reinforcement; P=applied axial force; P_0=nominal axial load capacity equal to $0.85f_c'(A_g - A_s) + f_y A_s$; A_s=area of longitudinal reinforcement; A_g=gross cross sectional area and h=total column depth. Note that the second term of Eq. (4) accounts for displacement due to the longitudinal reinforcement slipping out of joint or foundation. However, it is more reasonable to relate plastic hinge length only to flexural displacement (Bae and Bayrak 2008).

From the above-mentioned equations, five parameters are identified that are significant to the plastic hinge length, namely: axial force, shear span-to-depth ratio, longitudinal reinforcing ratio, concrete compressive strength and yield strength (material type) of longitudinal reinforcement. However, none of the above equations include all five parameters. In addition, existing expressions are not applicable to reinforced concrete members with USD 685 reinforcing bars, a new type of reinforcing bar that has a yield strength of 685 MPa (100 ksi) and has attracted increasing interest in recent years.

This paper examines the plastic hinge length of circular reinforced concrete columns using a three-dimensional (3D) finite element method (FEM). The parameters investigated are longitudinal reinforcing ratio, shear span-to-depth ratio, axial force ratio and concrete compressive strength. Two yield strengths, 414 MPa (60 ksi) and 685 MPa (100 ksi), are considered for longitudinal reinforcement. Simplified formulas are proposed for determining the plastic hinge length of circular reinforced concrete columns.

2. Three-dimensional finite element method

2.1 General description

As the cost of computational power decreases, the use of 3D FEM in reinforced concrete members has been growing in recent years (e.g. Hara 2011, Ou *et al.* 2007, Xiaoran and Yuanfeng 2010). This research uses *ABAQUS* (HKS 2006) to develop a non-linear 3D FEM for modeling the behavior of reinforced concrete columns under combined axial and lateral forces. Test results of column specimens 415 and 430 examined by Lehman and Moehle (2000) were used to validate the finite element method. Column 415 had an aspect ratio of 4 and a longitudinal reinforcing ratio of 1.5%. Column 430 had an aspect ratio of 4 and a longitudinal reinforcing ratio of 3%. The finite element model of the specimen consisted of a thin plate, a column and a foundation, as illustrated in Fig. 1.

The concrete portion of the column and cap beam was modeled by eight-node solid elements with a reduced-integration scheme (C3D8R) (Fig. 2a). The steel reinforcement was modeled using two-node truss elements (T3D2) (Fig. 2b). The bond-slip behavior of longitudinal reinforcement relative to the foundation was modeled by the concept of equivalent unbonded length (Ou *et al.* 2010). The

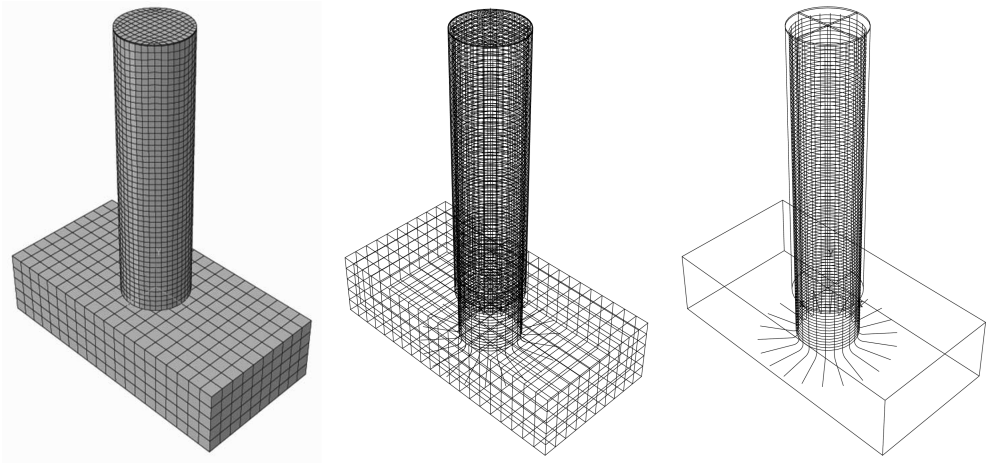

Fig. 1 3D finite element model

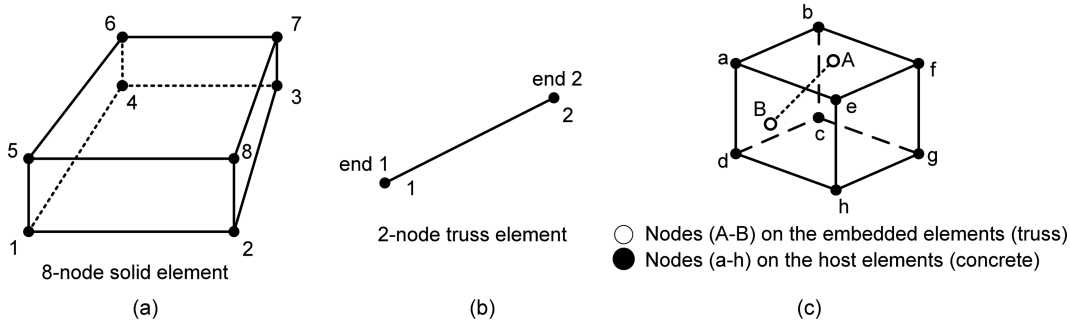

Fig. 2 (a) 8-node element (C3D8R), (b) truss element (T3D2) and (c) embedded constraint

size of the mesh of longitudinal reinforcement in the foundation was equal to $6d_b$. The truss elements were embedded in and fully bonded to the solid elements (Fig. 2c). The thin plate on top of the column acted as a force transfer plate, modeled with C3D8R rigid plate and tied to the top of the column. The model was subjected to a constant gravity load first, modeled as uniform load on the top of the plate. Lateral displacement was subsequently applied at mid-height of the thin plate. Base shear was calculated by summing the horizontal reaction forces at the base. The model for column 415 had a total of 35442 nodes.

2.2 Material models

A damaged concrete plasticity model with unconfined concrete behavior was used to model the concrete in compression. Mander's unconfined model (Mander *et al.* 1988) was used for normal-strength concrete (30~45 MPa). Collins model (Collins *et al.* 1993) was applied for high-strength concrete (>45 MPa).

All the compression stress-strain relationships are illustrated in Fig. 3(a). The truss elements representing the transverse reinforcement naturally generated a confining effect on the core concrete which exhibited confined concrete behavior during analysis. An average tensile stress-strain model for concrete proposed by Belarbi and Hsu (1994) was used to account for the tension stiffening

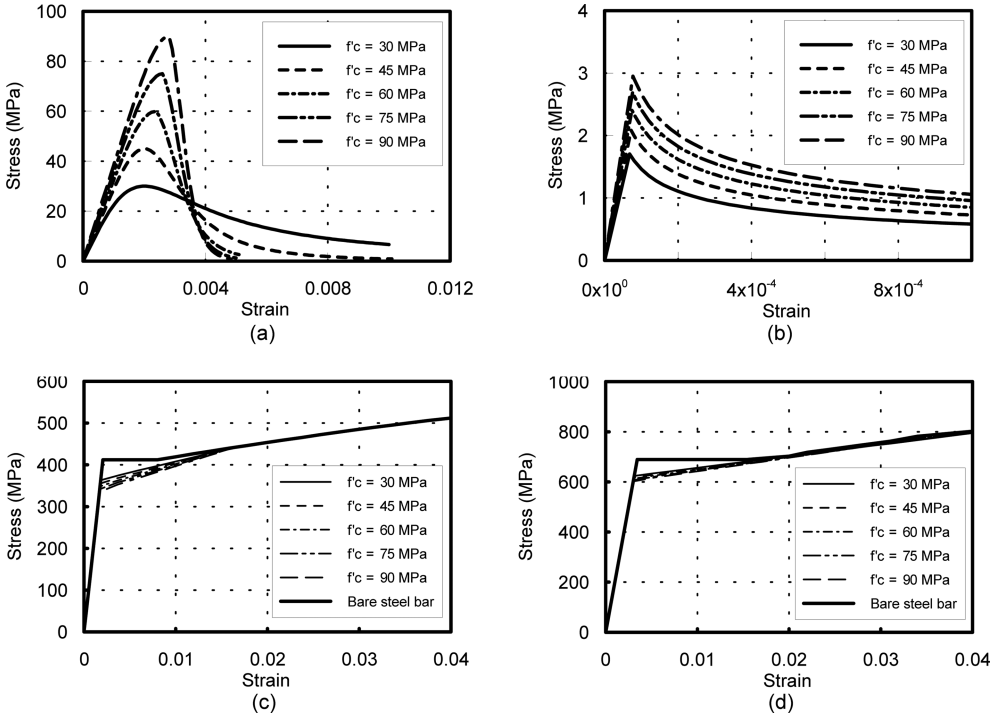

Fig. 3 Material stress-strain relationships: (a) concrete in compression, (b) concrete in tension, (c) 414 MPa rebar and (d) 685 MPa rebar

effect. The resulting stress-strain curves are illustrated in Fig. 3(b). In addition, a modified stress-strain model for steel reinforcement proposed by Belarbi and Hsu (1994) was adopted, with the resulting stress-strain curves illustrated in Figs. 3(c) and 3(d) for respective yield strengths of 414 MPa and 685 MPa. The 685 MPa stress-strain curve was obtained from a tension coupon test of a USD 685 reinforcing bar.

3. Validation

3.1 Column design

General design information about column specimens 415 and 430 is listed in Table 1.

3.2 Average curvature and shear rotation

The average curvature and shear rotation along the column were approximated using Eqs. (6) and (7) (Lehman and Moehle 2000), respectively and illustrated in Fig. 4.

$$\phi = \frac{\Delta S - \Delta N}{bh} \tag{6}$$

Table 1 General design information of columns 415 and 430

Parameter	Column 415	Column 430
Shear span-to-depth ratio (L/h)	4	4
Longitudinal reinforcing ratio (A_s/A_g)	1.5%	3%
Concrete compressive strength (f_c')	30 MPa	32 MPa
Concrete tension strength (f_t')	2.9 MPa	3.2 MPa
Yield strength of longitudinal reinforcement (f_y)	510 MPa	510 MPa
Ultimate strength of longitudinal reinforcement (f_u)	680 MPa	680 MPa
Volumetric ratio of transverse reinforcement (ρ_s)	0.7%	0.7%
Vertical spacing of transverse of reinforcement (s_o)	32 mm	32 mm
Axial load (P)	654 kN	654 kN

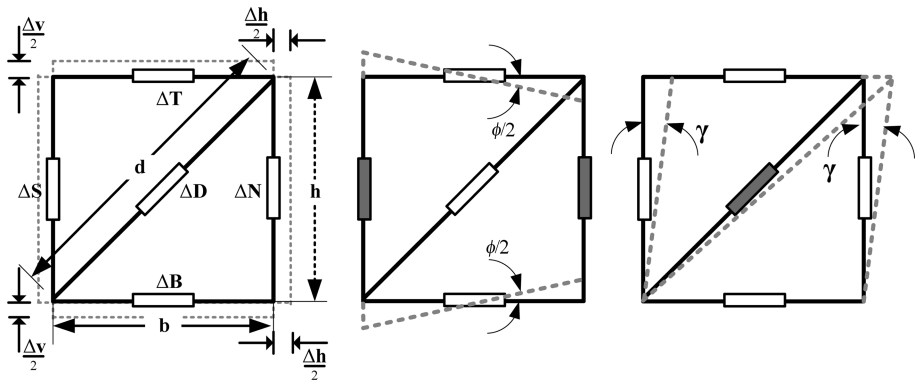

Fig. 4 Average curvature and average shear rotation along the member

$$\gamma = \frac{\sqrt{(d+\Delta D)^2-(h+\Delta_v)^2}-(b+\Delta h)}{h+\Delta_v} \tag{7}$$

where ϕ and γ=average curvature and average shear strain, respectively; and b, d and h= horizontal, diagonal and vertical lengths, respectively; ΔN and ΔS=north and south vertical deformations, respectively; ΔT and ΔB=top and bottom horizontal deformations, respectively; ΔD=diagonal deformation; and Δ_v and Δ_h=average of the two vertical deformations and average of the two horizontal deformations, respectively. The deformation was calculated based on the displacements of the corresponding nodes on the surface of the column.

3.3 Comparison between experimental and analysis results

Comparisons between experimental and finite element analysis results are shown in Fig. 5. Figs. 5(a) and 5(d), Figs. 5(b) and 5(e) and Figs. 5(c) and 5(f) show the base shear versus the displacement of the column top, average curvature distribution and average shear rotation for columns 415 and 430, respectively. Good agreement can be seen for these comparisons. Figs. 6(a) and 6(b) show the contour of strain along axis 2 at the end of simulation for columns 415 and 430, respectively. High strain values can be seen around the compression region at the base of the

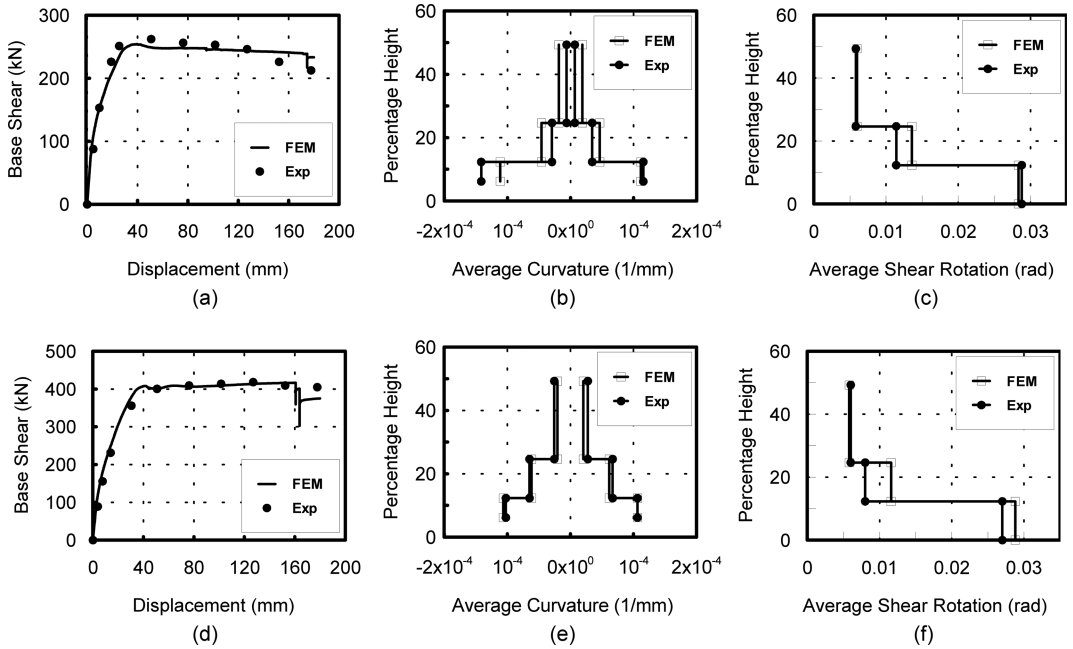

Fig. 5 Comparisons of results between experiment and FEM: base shear versus top displacement: (a) column 415 and (d) column 430; average curvature: (b) column 415 and (e) column 430; average shear rotation: (c) column 415 and (f) column 430

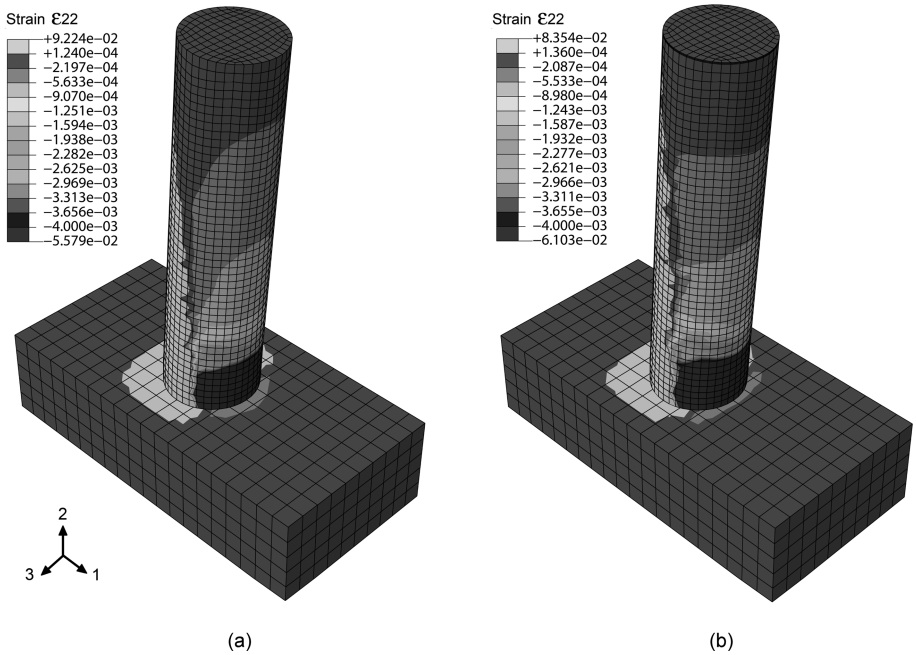

Fig. 6 Contour of strain along axis 2: (a) column 415 and (b) column 430

column. In the experiment, concrete damage occurred up to 305 mm and 330 mm from the base for columns 415 and 430, respectively. FEM result showed similar heights at 335 mm and 385 mm for columns 415 and 430, respectively, for the region exhibiting strains larger than the crushing strain. Both columns failed due to fracturing of the longitudinal reinforcement. The fracture strain was found to be approximately 4% from FEM.

4. Parametric study

4.1 Parameters

For each yield strength of longitudinal reinforcement (414 MPa and 685 MPa), four parameters were studied: axial load ratio P/P_o, shear span-to-depth ratio L/h, longitudinal reinforcing ratio A_s/A_g and concrete compressive strength f_c'. The axial load ratios were 0.05, 0.2, 0.3, 0.4 and 0.6. The shear span-to-depth ratios were 2, 4, 6, 8 and 10. The longitudinal reinforcing ratios were 1, 2, 3, 4 and 6%. The concrete compressive strengths were 30, 45, 60, 75 and 90 MPa. Each parameter had

Table 2 Taguchi *L*25 parametric combinations for each steel yield strength

No	P/P_o	L/h	A_s/A_g (%)	f_c' (MPa)
1	0.05	2	1	30
2	0.05	4	2	45
3	0.05	6	3	60
4	0.05	8	4	75
5	0.05	10	6	90
6	0.2	2	2	60
7	0.2	4	3	75
8	0.2	6	4	90
9	0.2	8	6	30
10	0.2	10	1	45
11	0.3	2	3	90
12	0.3	4	4	30
13	0.3	6	6	45
14	0.3	8	1	60
15	0.3	10	2	75
16	0.4	2	4	45
17	0.4	4	6	60
18	0.4	6	1	75
19	0.4	8	2	90
20	0.4	10	3	30
21	0.6	2	6	75
22	0.6	4	1	90
23	0.6	6	2	30
24	0.6	8	3	45
25	0.6	10	4	60

five discrete levels. All columns had a diameter of 600 mm.

The Taguchi robust design method has been shown to effectively assess the relative importance of design variables while reducing experimental effort (Dar *et al.* 2002, Fowlkes and Creveling 1995), and was used for parametric analysis in this study. Five levels of four parameters required the 25 design parametric combinations referred to as the $L25$ orthogonal array in the Taguchi method. Each yield strength of longitudinal reinforcement resulted in 25 parametric combinations, as listed in Table 2. Each parametric combination was designed with the minimum volumetric ratio ρ_s of transverse reinforcement as required by ACI 318 (2008) sections 10.9 and 21.6.4.

4.2 Definition of plastic hinge length

The top displacement Δ_{top} of a cantilever-reinforced concrete column consists of three components: (1) flexural displacement $\Delta_{flexure}$; (2) displacement due to fixed-end rotation resulting from longitudinal bars slipping out of joint or foundation Δ_{slip} and (3) shear displacement Δ_{shear}, and can be expressed as follows

$$\Delta_{top} = \Delta_{flexure} + \Delta_{slip} + \Delta_{shear} \tag{8}$$

The contribution of flexural deformations to the top displacement of a cantilever column can be computed by integrating curvatures (ϕ) over the height of the column (L).

$$\Delta_{flexure} = \int_0^L \phi(x) x\, dx \tag{9}$$

To simplify the calculation, the plastic curvature is assumed to be uniformly distributed over the plastic hinge length as illustrated in Fig. 7.

Based on this simplified curvature distribution, the plastic hinge length of a cantilever column can be obtained using the following equation.

$$\Delta_{flexure} = \Delta_y + \Delta_p = \left(\frac{\phi_y L}{2}\right)\left(\frac{2}{3}L\right) + (\phi_u - \phi_y) L_p (L - 0.5L_p) = \frac{\phi_y L^2}{3} + (\phi_u - \phi_y) L_p (L - 0.5L_p) \tag{10}$$

where Δ_y=yield displacement; Δ_p=plastic displacement; ϕ_u=ultimate curvature and ϕ_y=yield curvature. From Eq. (10), it can be seen that calculating the plastic hinge length requires the calculation of

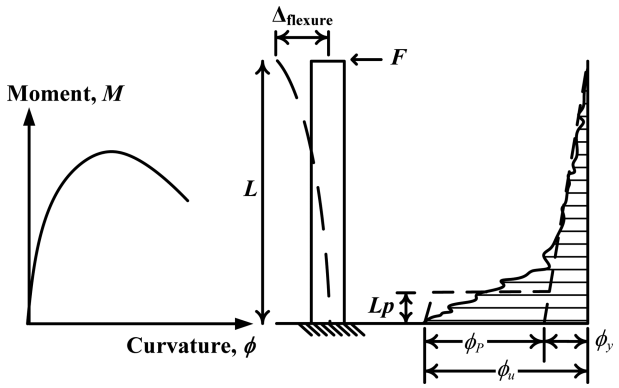

Fig. 7 Definition of plastic hinge length

three parameters: flexural displacement $\Delta_{flexure}$, yield curvature ϕ_y and ultimate curvature ϕ_u. The flexural displacement is calculated using Eq. (9) with curvature distribution computed by Eq. (6). Methods of determining the other two parameters are presented in the following sections.

4.3 Ultimate condition

A 20% force drop from the peak base shear was used as the first ultimate condition of the column as illustrated in Fig. 8(a). The second ultimate condition was related to rebar fracture (including buckling and fatigue effect) as defined when the peak rebar strain reached 0.04. This value of fracture strain was obtained from the above-mentioned verification study. Note that the strain could change depending on other factors such as loading history. The validity of using this criterion to determine the plastic hinge length will be further discussed in a later section "Plastic hinge length versus drift". The third ultimate condition was reached when the peak compressive strain of confined concrete reached the strain as defined Eq. (11) (Paulay and Priestley 1992).

$$\varepsilon_{cu} = 0.004 + \frac{1.4\rho_s f_{yh}\varepsilon_{sm}}{f'_{cc}} \tag{11}$$

where f_{yh} and ε_{sm} =yield strength and ultimate strain, 0.1, of the transverse reinforcement, respectively; f'_{cc} =ultimate confined concrete strength. The ultimate strain of confined concrete was calculated to be ranging from 1.9% to 2%.

4.4 Yield curvature

The yield curvature was obtained by extending the curvature distribution at the elastic region of a column with a straight line to the end of the inelastic region in the average curvature versus column height chart, as illustrated in Fig. 8(b). The curvature for this purpose was measured using the displacement of nodes of the extreme tension and compression longitudinal reinforcement. In Fig. 8(b), elastic curvature was plotted with a dashed line.

4.5 Ultimate curvature

Lehman and Moehle (2000), attached the first displacement transducer at 0.25h (h=depth of the

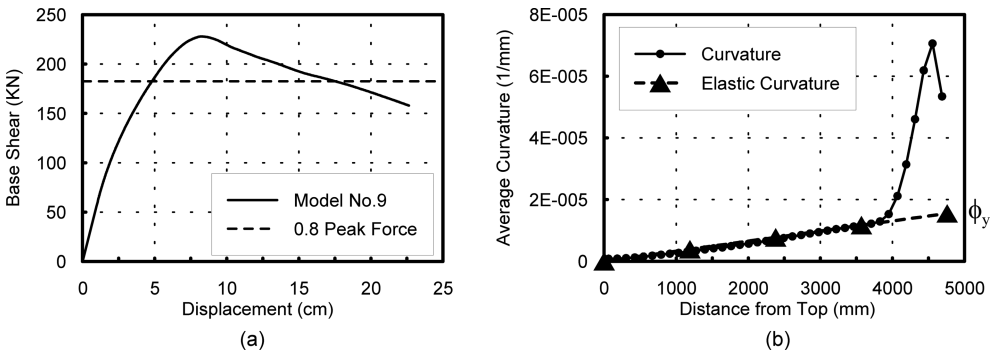

Fig. 8 (a) Definition of ultimate condition and (b) definition of yield curvature

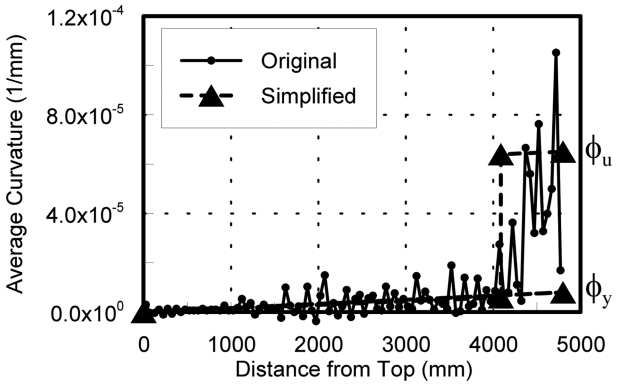

Fig. 9 Definition of ultimate curvature

column) from the base of the column to calculate the ultimate curvature. Thus the ultimate curvature was calculated using the average of the curvature values within the 0.25*h* region from the base of the column as illustrated in Fig. 9. It was found that the peak curvature value did not always occur in the base section of the column as shown in Fig. 9. This was also observed by Bae and Bayrak (2008).

5. Results and comparison

5.1 Plastic hinge length

With the above-mentioned definitions, Eq. (10) was solved for the plastic hinge length, which is listed in Table 3 for all parametric combinations and compared with Bae's formula as defined in Eq. (5) (Bae and Bayrak 2008). Table 3 shows significant differences occurred for the 414 MPa case in models 1, 2, 3 and 10. Close examination of Eq. (5) revealed that, for these models, the term in the square bracket ($0.3\ P/P_0 + 3A_s/A_g - 0.1$) of Eq. (5) gives a negative value or a value close to zero. This also happened in Bae's study (Bae and Bayrak 2008). For Bae's specimens S24-4UT and S24-5UT, both specimens were designed with P/P_0 equal to 0.2 and with A_s/A_g equal to 1.25%, resulting in a negative value of the term in the square bracket of Eq. (5). Therefore, for both specimens, the plastic hinge length was controlled by the lower limit of the Eq. (5), which is equal to 0.25*h*. However, the plastic hinge lengths were experimentally determined to be 0.49*h* and 0.47*h*, respectively. This phenomenon also occurred in column 415 where the finite element analysis gives a plastic hinge length equal to 0.53*h* while Bae's formula gives a plastic hinge length equal to 0.25*h*. In fact, Bae and Bayrak reported differences ranging from 3% to 40% between the plastic hinge lengths obtained from Eq. (5) and those obtained from their simplified analytical study. The differences between finite element analysis and Bae's formula in Table 3 may also be attributed to the fact that this research focuses only on 414 MPa longitudinal reinforcement, while Bae's formula was derived from a database with different values of yield strength. Note that for the 685 MPa cases, two models (Nos. 11 and 25) remained in the elastic range when the ultimate condition was reached.

Table 3 Plastic hinge lengths from FEM and from Eq. (5)

NO	414 MPa Longitudinal reinforcement				685 MPa Longitudinal reinforcement		
	L_p (mm) (FEM)	L_p (mm) (Bae's formula)	Difference	Failure mode*	L_p (mm) (FEM)	L_p/h	Failure mode*
1	249.74	150.00	66%	1	242.98	0.4	1
2	353.57	150.00	136%	1	330.99	0.55	1
3	345.42	165.24	109%	3	362.05	0.6	1
4	318.32	335.06	-5%	2	441	0.74	1
5	300.41	720.00	-58%	3	483.92	0.81	2
6	195.07	175.80	11%	1	373	0.62	2
7	276.39	267.52	3%	2	325.04	0.54	2
8	334.51	449.47	-26%	3	457.96	0.76	3
9	711.65	833.94	-15%	2	989.17	1.65	2
10	489.94	150.00	227%	3	557.45	0.93	3
11	196.13	244.76	-20%	3	-	-	3
12	440.32	421.65	4%	2	489.72	0.82	2
13	625.50	770.95	-19%	2	425.96	0.71	2
14	357.91	257.84	39%	3	666.55	1.11	3
15	533.47	459.00	16%	3	813.16	1.36	3
16	352.92	321.82	10%	2	284.53	0.47	3
17	593.50	635.97	-7%	3	435.87	0.73	2
18	298.70	338.88	-12%	3	498.95	0.83	3
19	364.91	541.20	-33%	3	652.88	1.09	3
20	672.66	803.80	-16%	3	1,189.22	1.98	3
21	475.11	464.98	2%	3	397.17	0.66	3
22	469.55	419.92	12%	3	584.5	0.97	3
23	585.93	659.40	-11%	3	699.14	1.17	3
24	613.48	961.04	-36%	3	970.53	1.62	3
25	746.21	1369.12	-45%	3	-	-	3

*1: fracture of rebar, 2: crushing of confined concrete and 3: P-Δ effect.

5.2 Plastic hinge length versus drift

Fig. 10(a) shows the relationship between plastic hinge length and drift for column model No. 9 with 414 MPa longitudinal reinforcement. Plastic hinge length was equal to zero at initial loading when the condition was related to elastic response in the longitudinal rebar. When longitudinal rebar began to yield as shown in Fig. 10(b), plastic hinge length increased as the drift increased, saturating after drift reached a certain value. For this case, plastic hinge length remained approximately constant at around 710 mm after reaching a drift equal to 1.5% until the ultimate drift (3.65%), indicating that the value of plastic hinge length is approximately constant near the ultimate condition. Thus, plastic hinge length is not sensitive to changes in the criteria used to define the three ultimate conditions adopted in this research.

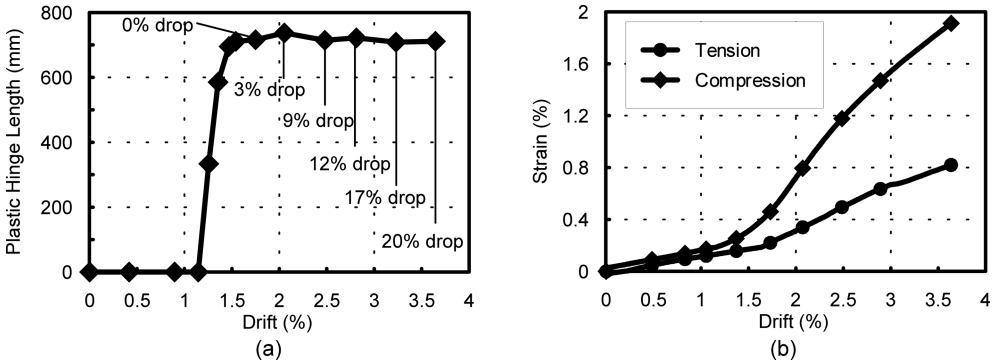

Fig. 10 (a) Drift versus plastic hinge length (Model No. 9, 414 MPa case) and (b) drift versus the strain of extreme longitudinal reinforcement

6. Proposed formulas for plastic hinge length

6.1 Proposed formulas

Based on the results of finite element analysis, linear relationships between the parameters examined (P/P_o, L/h, f_c' and A_s/A_g) and the plastic hinge length were used to simplify calibration of the plastic hinge length expression. By using least-squares regression analyses, values in Table 3 were inputted to construct new formulas for plastic hinge length. The formula for longitudinal reinforcement with yield strength of 414 MPa is shown in the following equation and the regression statistics are listed in Table 4.

$$\frac{L_p}{h} = 0.936\left(\frac{P}{P_0}\right) + 7.398\left(\frac{A_s}{A_g}\right) + 0.06\left(\frac{L}{h}\right) - 0.003(f_c') \quad (f_c' \text{ in MPa}) \tag{12}$$

Based on the regression statistics, the value of multiple R, R square, and adjusted R square are above 90%, which means this proposed formula closely matches with the results of finite element analysis. The differences of plastic hinge length obtained from the finite element analysis, Bae's formula, and proposed formula are illustrated in Fig. 11(a). The formula for longitudinal reinforcement with yield strength of 685 MPa is shown in the following equation and the regression statistics are listed in Table 5.

$$\frac{L_p}{h} = 0.503\left(\frac{P}{P_0}\right) + 3.218\left(\frac{A_s}{A_g}\right) + 0.053\left(\frac{L}{h}\right) + 0.0018(f_c') \quad (f_c' \text{ in MPa}) \tag{13}$$

Table 4 Regression statistics for the 414 MPa case

Regression statistics		Coefficients	
Multiple R	98.57%	P/P_0	0.935503
R Square	97.17%	A_s/A_g	7.397764
Adjusted R square	93.00%	L/h	0.060694
Standard error	0.143	f_c'	-0.00305

Table 5 Regression statistics for the 685 MPa case

Regression statistics		Coefficients	
Multiple R	97.55%	P/P_0	0.502501245
R Square	95.16%	A_s/A_g	3.218313562
Adjusted R square	89.13%	L/h	0.05322844
Standard error	0.174	f_c'	0.001769133

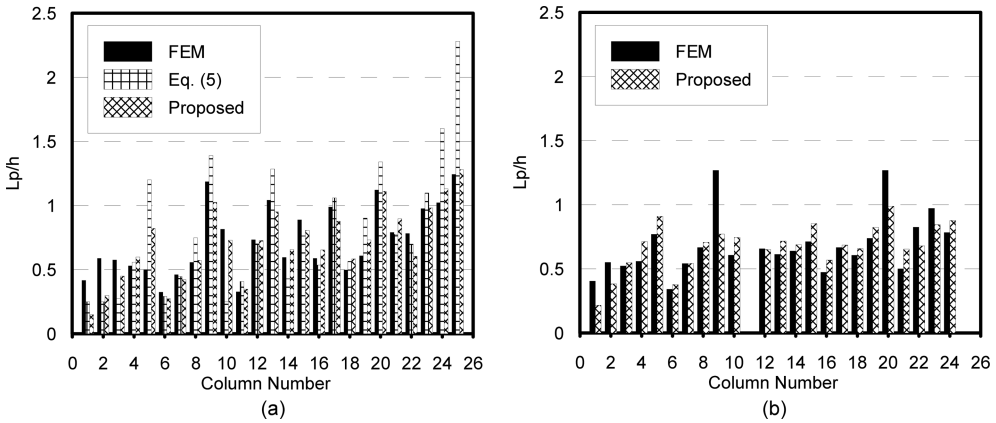

Fig. 11 Comparisons of plastic hinge length: (a) longitudinal reinforcement with a yield strength of 414 MPa and (b) longitudinal reinforcement with a yield strength of 685 MPa

The regression statistics show that the proposed formula closely matches the finite element results. The differences of plastic hinge length obtained from the finite element analysis and proposed formula are illustrated in Fig. 11(b).

7. Discussion

7.1 Effect of axial load ratio (P/P_0)

Previous experiments (Baker 1956, SakaiI and Sheikh 1989, Bae and Bayrak 2008) have shown that the plastic hinge length increased with the ratio of axial load. The same trend was observed for the proposed formulas, in which a positive coefficient of P/P_0 means that an increase in the axial load ratio will result in an increase of the plastic hinge length. Increasing the axial load ratio increases the extent of crushing and spalling of cover concrete at the base of the column. A larger crushed and spalled region means that the compression longitudinal reinforcement has to take more compression force. As a result, the plasticity of longitudinal reinforcement will spread further and the plastic hinge length will increase as a result of the increase of plastic area. Fig. 12 shows the effect of axial loads ranging from $0.05P_0$~$0.6P_0$ for the 414 MPa (Fig. 12a) and for the 685 MPa (Fig. 12b) cases for A_s/A_g=1% and f_c' =30 MPa. Comparing Figs. 12(a) and 12(b) shows that most cases show a lower value of plastic hinge length when yield strength increases from 414 MPa to 685 MPa. Some, however, show an opposite trend. For example, the 685 MPa case with L/h=2 and P/P_0=0.05 results a plastic hinge length longer than that of the 414 MPa case.

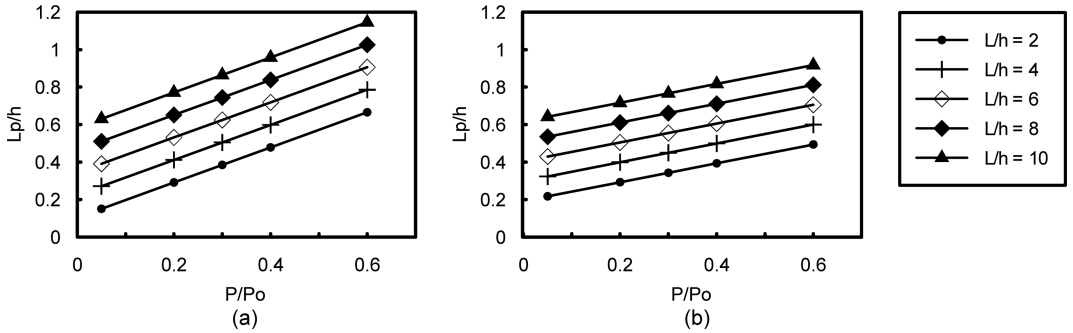

Fig. 12 Relationship between plastic hinge length and axial load ratio for different shear span-to-depth ratio: (a) 414 MPa case and (b) 685 MPa case

7.2 Effect of longitudinal reinforcing ratio (A_s/A_g)

Corley (1966), Mattock (1964) and Mendis (2001) have taken A_s/A_g into account in their proposed formulas for plastic hinge length. However, all of their formulas were derived from beam tests rather than from column tests. Bae and Bayrak (2008) conducted column tests and included A_s/A_g in the proposed formula (Eq. 5). According to the formula, plastic hinge length trends higher as the longitudinal reinforcing ratio increases. The proposed formulas in this research show an ascending trend as illustrated in Figs. 13(a) and 13(b) for the 414 MPa and 685 MPa cases, respectively, for L/h=4 and f_c' =30 MPa.

This trend can be explained as follows; when a concrete column without any longitudinal reinforcement is subjected to axial and lateral loads, one large crack will occur at the base and result in a very short plastic hinge length. Adding longitudinal reinforcement will increase the number and extent of the cracks due to the bond between concrete and longitudinal reinforcement, which causes spread of plasticity in the longitudinal reinforcement. The increased size of the plastic region leads to a longer plastic hinge length.

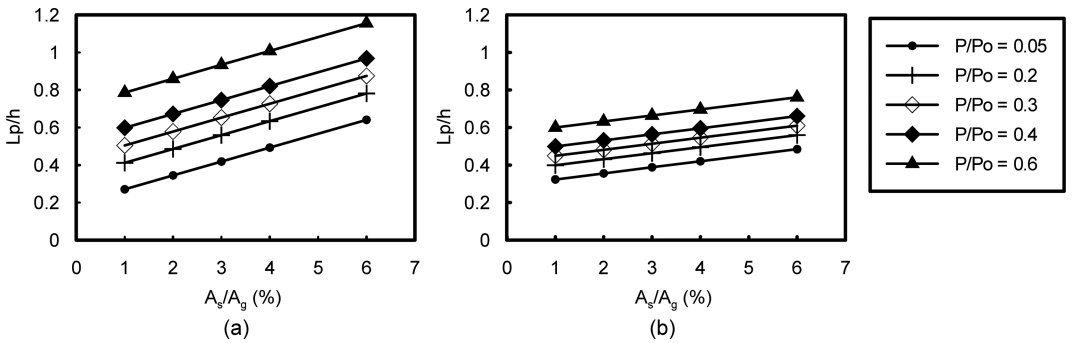

Fig. 13 Relationship between plastic hinge length and longitudinal reinforcing ratio for different levels of axial load ratio: (a) 414 MPa case and (b) 685 MPa case

7.3 Effect of shear span-to-depth ratio (L/h)

The proposed formulas show that plastic hinge length increases with *L/h*, as illustrated in Fig. 14 for a column with a fixed axial load ratio equal to 0.3 and a concrete strength equal to 60 MPa. This observation is consistent with Bae's formula (Eq. 5). It can be explained as follows: a column with a larger shear span-to-depth ratio has the same values of ultimate moment and yield moment as a column with the same sectional design but with a smaller shear span-to-depth ratio. However, the moment gradient is lower for the column with a larger shear span-to-depth ratio. As a result, the yield region is larger and, hence, the plastic hinge length is longer. A similar slope for both cases indicates similar coefficients were applied in front of *L/h* (0.06 for the 414 MPa case and 0.053 for the 685 MPa case), and that increasing yield strength has little effect on the slope of the trend.

7.4 Effect of concrete strength on plastic hinge length

As shown in Fig. 15, plastic hinge length can increase or decrease as concrete strength increases for various shear span-to-depth ratios. For the 414 MPa case shown in Fig. 15(a), plastic hinge length decreases as concrete strength increases. This observation is consistent with test results of specimens S24-4UT and S24-5UT (Bae and Bayrak 2008), as shown in Table 6. The plastic hinge length of specimen S24-4UT, which had a lower concrete strength, was experimentally determined

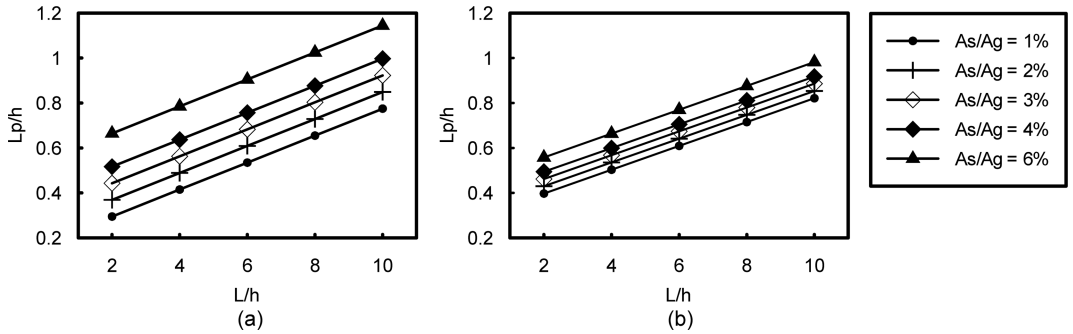

Fig. 14 Relationship between plastic hinge length and shear span-to-depth ratio for different levels of longitudinal reinforcing ratio: (a) 414 MPa case and (b) 685 MPa case

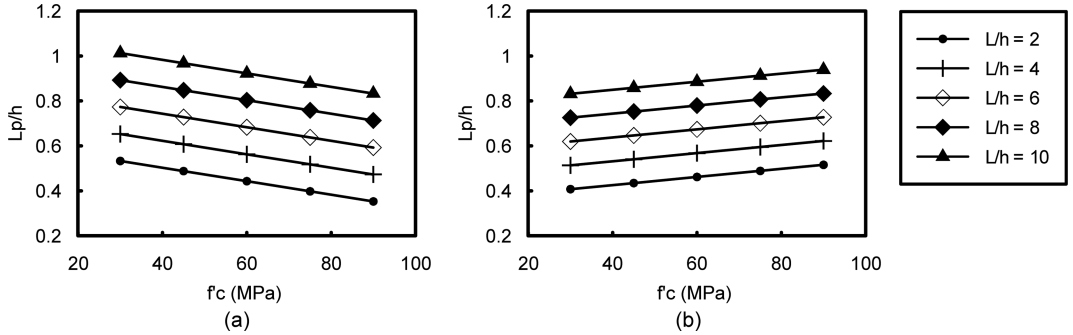

Fig. 15 Relationship between plastic hinge length and concrete strength for different levels of shear span-to-depth ratio: (a) 414 MPa case and (b) 685 MPa case

Table 6 Comparisons between proposed formula, experiment and Eq. (5)

Column	P/P_0	A_s/A_g (%)	L/h	f_c' (MPa)	L_p/h Proposed	L_p/h Experiment	L_p/h (Eq. 5)
S24-2UT	0.5	1.25	5	43.4	0.69	0.66	0.69
S17-3UT	0.5	1.25	7	43.4	0.82	0.91	0.86
S24-4UT	0.2	1.25	5	36.5	0.471	0.49	0.25
S24-5UT	0.2	1.25	5	41.4	0.456	0.47	0.25

Table 7 Column models for verification

Column	f_y (MPa)	P/P_0	A_s/A_g	L/h	f_c' (MPa)
1	414	0.2	4%	6	30
2	414	0.2	4%	6	60
3	685	0.2	4%	6	30
4	685	0.2	4%	6	60
5	414	0.2	2%	4	30
6	414	0.2	2%	4	60
7	685	0.2	2%	4	30
8	685	0.2	2%	4	60

to be greater than that of S24-5UT. Table 6 also shows that the plastic hinge lengths determined by the proposed formula (Eq. 12) for the two specimens are quite similar to the experimental values while, as previously mentioned, Bae's formula (Eq. 5) makes significantly different predictions. For the other two specimens, S24-2UT and S17-3UT, tested by Bae and Bayrak (2008), both Bae's formula and proposed formula give similar plastic hinge lengths close to experimentally determined values.

However, for the 685 MPa case, Fig. 15(b) shows that plastic hinge length increases with concrete strength, unlike for the 414 MPa case. An explanation for this difference requires a detailed discussion of every part of the formula. Eight column models with design parameters as listed in Table 7 were used to investigate the effect of concrete strength on the plastic hinge length and to further verify the proposed plastic hinge length formulas. The parameters listed in Table 7 were

Table 8 FEM results and comparison with proposed formulas and Eq. (5)

Column	L_p/h proposed	L_p/h FEM	L_p/h Eq. 5	ϕ_y (1/mm)	Δ_y (mm)	ϕ_u (1/mm)	Δ_{flex} (mm)	Failure mode*	$\phi_u-\phi_y$ (1/mm)	$\Delta_{flex}-\Delta_y$ (mm)
1	0.753	0.762	0.73	7.95E-06	34.34	5.84E-05	112.15	2	5.05E-05	77.80
2	0.663	0.635	0.73	7.50E-06	32.40	4.47E-05	80.69	3	3.72E-05	48.29
3	0.601	0.580	0.73	1.60E-05	69.12	5.41E-05	114.57	2	3.81E-05	45.45
4	0.655	0.678	0.73	1.15E-05	49.68	5.44E-05	108.92	2	4.29E-05	59.24
5	0.485	0.516	0.33	8.00E-06	15.36	7.15E-05	59.46	2	6.35E-05	44.10
6	0.395	0.483	0.33	7.50E-06	14.40	3.29E-05	31.01	3	2.54E-05	16.61
7	0.431	0.515	0.33	1.20E-05	23.04	5.19E-05	50.74	2	3.99E-05	27.70
8	0.485	0.600	0.33	1.00E-05	19.20	4.20E-05	44.78	3	3.20E-05	25.58

*1: fracture of rebar, 2: crushing of confined concrete and 3: P-Δ effect.

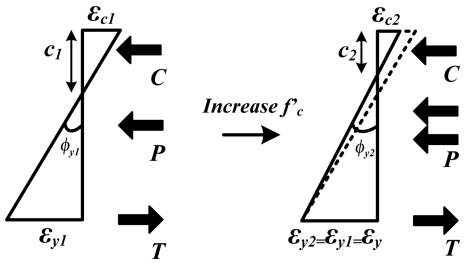

Fig. 16 Sectional analysis at yield condition

chosen to be different from the Taguchi parametric combinations as listed in Table 2. Note that to keep the axial load ratio P/P_0 constant, axial force P will increase as f_c' increases. Table 8 shows the analysis results of the eight columns.

Fig. 16 shows the sectional strain diagram at the yield condition. Increasing f_c' not only increases concrete stress in the compression region but also the axial force due to the increase of P_0, $0.85f_c'(A_g-A_s)+f_y A_s$. The increased stress reduces the neutral axis depth c while the increased axial force increases it. Due to the presence of $f_y A_s$ in P_0, the axial force does not increase as quickly as f_c'. The combined effect results in a smaller neutral axis depth and smaller extreme compression fiber strain ($c_2<c_1$ and $\varepsilon_{c2}<\varepsilon_{c1}$), as illustrated in Fig. 16. Since the yield strain is constant ($\varepsilon_{y1}=\varepsilon_{y2}=\varepsilon_y$), a smaller neutral axis depth makes the yield curvature smaller ($\phi_{y2}<\phi_{y1}$) and contributes to a smaller yield displacement Δ_{yield}. This is confirmed by simulation results of all four pairs of columns in Table 8. For example, the yield displacement of column 1, which was designed with a lower concrete strength, was found to be higher than that of column 2. For the ultimate condition, increasing f_c' may increase or decrease the ultimate curvature depending on the failure mode. For columns 3 and 4, the failure mode is the crushing of confined concrete. Increasing f_c', and hence concrete stress, in the compression region reduces the neutral axis depth but not as much as the yield condition since, as show in Fig. 3, the stress on higher-strength concrete drops more quickly after reaching its peak stress. Increasing f_c' also increases axial force, which increases the neutral axis depth. The combined effect results in a slight decrease of the neutral axis depth. Since the ultimate strain of the confined concrete is similar among the columns examined, a decrease of the neutral axis depth results in an increase of the ultimate curvature. For the other columns, increasing f_c' causes the failure mode to shift from the crushing of confined concrete to a 20% drop in strength due to a more severe P-Δ effect caused by a higher axial load. For these columns, the ultimate curvature decreases as expected.

Eq. (10) can be rearranged as Eq. (14). Based on Table 8, for the 414 MPa case at ultimate condition, the decrease of the left side ($\Delta_{flexure}-\Delta_{yield}$) of Eq. (14) is faster than the curvature capacity ($\phi_u-\phi_y$) in the right side of Eq. (14) when f_c' is increased. To balance this condition, plastic hinge length should be decreased. On the other hand, for the 685 MPa case, the decrease of the curvature capacity ($\phi_u-\phi_y$) in right side of Eq. (14) is faster than ($\Delta_{flexure}-\Delta_{yield}$) in the left side of Eq. (14). To balance this condition, plastic hinge length should be increased. This phenomenon, illustrated in Fig. 17, explains why different trends were observed between the two yield strength cases in Fig. 15.

$$\Delta_{flexure}-\Delta_{yield}=(\phi_u-\phi_y)L_p(L-0.5L_p) \tag{14}$$

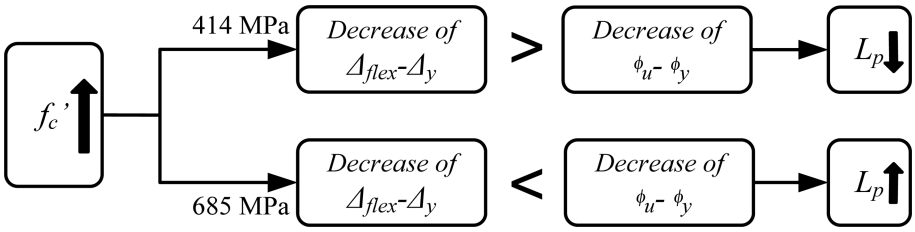

Fig. 17 Flowchart of plastic hinge length affected by concrete strength

Table 8 further confirms that change of the concrete strength and yield strength of the longitudinal reinforcement will alter the plastic hinge length.

8. Conclusions

This study presents the following main conclusions:

1. From the validation process, it is shown that the developed finite element method can provide a satisfactory prediction of the behavior of reinforced concrete columns under combined axial and lateral loads in terms of base shear versus displacement, curvature along the member and shear rotation along the member.
2. Simplified formulas listed below for estimating the plastic hinge length of circular reinforced concrete columns for longitudinal reinforcement with yield strengths of 414 MPa and 689 MPa are proposed and validated.

For longitudinal reinforcement with yield strength of 414 MPa

$$\frac{L_p}{h} = 0.936\left(\frac{P}{P_0}\right) + 7.398\left(\frac{A_s}{A_g}\right) + 0.06\left(\frac{L}{h}\right) - 0.003(f_c') \quad (f_c' \text{ in MPa})$$

For longitudinal reinforcement with yield strength of 685 MPa

$$\frac{L_p}{h} = 0.503\left(\frac{P}{P_0}\right) + 3.218\left(\frac{A_s}{A_g}\right) + 0.053\left(\frac{L}{h}\right) + 0.0018(f_c') \quad (f_c' \text{ in MPa})$$

3. Through a parametric study, it is found that increasing the axial load ratio, longitudinal reinforcing ratio and shear span-to-depth ratio will increase the plastic hinge length in both the 414 MPa and 685 MPa cases. Increasing concrete strength will decrease the plastic hinge length for the 414 MPa case while increase it for the 685 MPa case. Mechanical explanations on these observations are presented and discussed.

Acknowledgements

The authors would like to thank the National Science Council of the Republic of China, Taiwan, for financially supporting this research under Contract No. NSC 99-2221-E-011-160.

References

ACI Committee 318. (2008), *Building code requirements for structural concrete (ACI 318-08) and commentary (ACI 318R-08)*, American Concrete Institute, Farmington Hills, MI, U.S.A.

Bae, S. and Bayrak, O. (2008), "Plastic hinge length of reinforced concrete columns", *ACI Struct. J.*, **105**(3), 290-300.

Baker, A.L.L. and Amarakone, A.M.N. (1964), "Inelastic hyper static frame analysis", *Flex. Mech. Reinf. Concrete ACI*, **12**, 85-142.

Belarbi, A. and Hsu, T.T.C. (1994), "Constitutive laws of concrete in tension and reinforcing bars stiffened by concrete", *ACI Struct. J.*, **91**(4), 465-474.

Collins, M.P., Mitchell, D. and MacGregor, J.G. (1993), "Structural design consideration for high-strength concrete", *ACI Struct. J.*, **15**(5), 27-34.

Corley, W.G. (1966), "Rotational capacity of reinforced concrete beams", *J. Struct. Div.-ASCE*, **92**(5), 121-146.

Dar, F.H., Meankin, J.R. and Aspden, R.M. (2002), "Statistical methods in finite element analysis", *J. Biomech*, **35**(9), 1155-1161.

Fowlkes, W.Y. and Creveling, C.M. (1995), *Engineering methods for robust product design using Taguchi methods in technology and product development*, Addison-Wesley.

Hara, T. (2011), "Application of computational technologies to R/C structural analysis", *Comput. Concrete*, **8**(1), 97-110

HKS. (2006), *ABAQUS user's manual Version 6.6*, Hibbitt, Karlsson & Sorensen, Inc, Pawtucket, RI, U.S.A.

Lehman, D.E. and Moehle, J.P. (2000), *Seismic performance of well-confined concrete bridge columns*, Pacific Earth. Eng. Res. Center, 1998-2001.

Mander, J.B., Priestley, M.J.N. and Park, R. (1988), "Theoretical stress-strain model for confined concrete", *J. Struct. Eng.-ASCE,* **114**(8), 1804-1826.

Mattock, A.H. (1964), "Rotational capacity of hinging regions in reinforced concrete beams", *Flex. Mech. Reinf. Concrete*, **12**, 143-181.

Mattock, A.H. (1967), "Discussion of rotational capacity of hinging regions in reinforced concrete beams", *J. Struct. Div.-ASCE,* **93**(2), 519-522.

Mendis, P. (2001), "Plastic hinge lengths of normal and high-strength concrete in flexure", *Adv. Struct. Eng.*, **4**(4), 189-195.

Ou, Y.C., Chiewanichakorn, M., Aref, A.J. and Lee, G.C. (2007), "Seismic performance of segmental precast unbonded post-tensioned concrete bridge columns", *J. Struct. Eng.-ASCE,* **133**(11), 1636-1647.

Ou, Y.C., Wang, P.H., Tsai, M.S., Chang, K.C. and Lee, G.C. (2010), "Large-scale experimental study of precast segmental unbonded post-tensioned concrete bridge columns for seismic regions", *J. Struct. Eng.-ASCE,* **136**(3), 255-264.

Paulay, T. and Priestley, M.J.N. (1992), *Seismic design of reinforced concrete and masonry buildings*, John Wiley and Sons, New York, U.S.A.

SakaiI, K. and Sheikh, S.A. (1989), "What do we know about confinement in reinforced concrete columns? (A critical review of previous work and code provisions)", *ACI Struct. J.*, **86**(2), 192-207.

Xiaoran, L. and Yuanfeng, W. (2010), "Three-dimensional nonlinear finite element analysis of reinforced concrete structures based on ANSYS program", *2nd Int. Conference on Computer Eng. Tech. (ICCET)*, **6**, 42-46.

CC